
ORTHOGAN: HIGH-PRECISION IMAGE GENERATION FOR TEETH ORTHODONTIC VISUALIZATION

Shen Feihong

Jilin University
gregoryfeihong@gmail.com

Liu jingjing

Zhejiang University
12221107@zju.edu.cn

Lou jianwen

Zhejiang University
jianwen.lou@zju.edu.cn

Li Haizhen

Shanghai Jiao Tong University School of Medicine
569286671@qq.com

Bing Fang

Shanghai Jiao Tong University School of Medicine
fangbing@sjtu.edu

Ma Chenglong

Zhejiang University
mchenglong@chohotech.com

Jin Hao

Harvard University
jinhao@g.harvard.edu

Yang Feng

Angelalign Research Institute
fengyang@angelalign.com

Zheng Youyi

Zhejiang University
youyizheng@zju.edu.cn

ABSTRACT

Aligning the teeth of a face image with a specified teeth shape is crucial in orthodontic treatment visualization. This task falls within the realm of conditional image editing, an area that has witnessed numerous methodological advancements in recent years. Despite this progress, existing methods face challenges in preserving the identity of the original teeth, particularly influenced by factors such as 3D teeth shape and lighting conditions. To tackle this issue, we introduce a novel style-based generative model designed to synthesize identity-preserving teeth images. Our model takes a user's frontal smile face image and their 3D scanned teeth model as input. It then transforms the 3D model into multi-modal conditions, including a binary mask, contour image, and depth map. The model outputs a face image with teeth that match the given 3D scan while aligning with the original image's contextual identity. The proposed method surpasses state-of-the-art teeth alignment techniques, exhibiting improved visual quality. Moreover, a rigorous user study, involving both doctors and patients, provides compelling evidence of the superior performance of the proposed method.

Keywords Deep Learning, Computer simulation, teeth alignment

1 Introduction

Teeth alignment of the frontal smile face is getting more and more attention [17, 47]. Patients who choose invisible teeth alignment have the willingness to know the effects of teeth alignment in different treatment stages. The natural goal of this task is to replace the teeth region of the smile face images with the generated teeth images. Different from other inpainting tasks [99], the generated teeth images in this task should be strictly aligned with the patient's actual 3D teeth model and have the natural outlooks simultaneously. Due to the complicated data formation in this task, the previous works [17] also fail to efficiently generate an aligned frontal smile image with high quality. Therefore, an accurate and efficient framework that can automatically predict high-quality smile simulation in photographs is needed for orthodontic visualization.



Figure 1: The result from popular diffusion-based text-to-image softwares. We set the same prompt and provide the same input if the software contains the inpainting or img2img function.

Orthodontic visualization mainly includes two sub-tasks: the pose fitting of scanned 3D teeth models and the generation of face images in the region of interest. The solutions of these two sub-tasks in previous work [17] contain irrational structures, thereby leading to relatively low accuracy and suboptimal outcomes. In this paper, we introduce novel approaches to address these issues. Specifically, we leverage differentiable rendering on the pose fitting stage and transfer the aligned 3D data to other modalities, including 2D teeth silhouette, depth image, and label mask. Our framework efficiently makes good use of these modalities to generate high-quality teeth images with our synthesis component. It should be noted that, in this paper, we do not include the content of 3d teeth auto-alignment.

The most essential part of alignment visualization is partial face image manipulation. Diffusion models [67, 68, 69] have demonstrated the ability to generate high-fidelity human face images. While several works propose some methods to reduce the inference speed and add controllable generating conditions, like ControlNet [89], most of these models require a large number of iterations to generate face images and a higher order of magnitude of training resources compared to style-based generation models. In figure 1, we test some public image-to-image models, and the results are not suitable for clinical applications. Similar to previous work[17], we introduce an adversarial mechanism and novel training method to our synthesis model *OrthoGAN*. Instead of the diffusion model, in the last decade, generative adversarial networks (GAN) have been utilized in many real-world applications [42, 10] and have achieved state-of-the-art performances. Many architectures of the GAN have been proposed to improve the fidelity and diversity of the generated signal including WGAN [41], BigGAN [10] et al. In recent years, StyleGAN [8] has been known for its ability to generate realistic images in various domains. EditGAN [11] applied it to generate realistic facial images, which allow users to edit images by modifying highly detailed part segmentation masks. Inspired by the success of multi-modal GAN [22], we propose our *OrthoGAN* network based on the style generation method, which combines the teeth geometry information from the 3D model and teeth visual characteristics from the RGB image to generate the corresponding after-treatment smile face photograph. Specifically, our novel architecture in the network structure and training method enables the model to fit the slight edge in input maps and the customized style-based architecture in our network allows the model to simulate complicated illumination conditions [100] on the faces of the teeth surpassing the former performance.

In summary, our main contributions are:

- We introduce differentiable rendering to the pose fitting of the 3D teeth model and surpass the performance of the previous method in both efficiency and accuracy. In particular, our edge-rendering-based fitting can be used on other fitting tasks that have object occlusion or lack RGBD feature information.
- We design a new conditional generation model to achieve teeth alignment visualization in the oral domain. It guarantees generation fidelity with a relatively small size and fast speed. This architecture can be applied to other conditional inpainting tasks that involve time series inputs.

2 Related Works

In this section, we review the previous research in the areas of differentiable rendering, and human face manipulation, which are highly related to our problem.

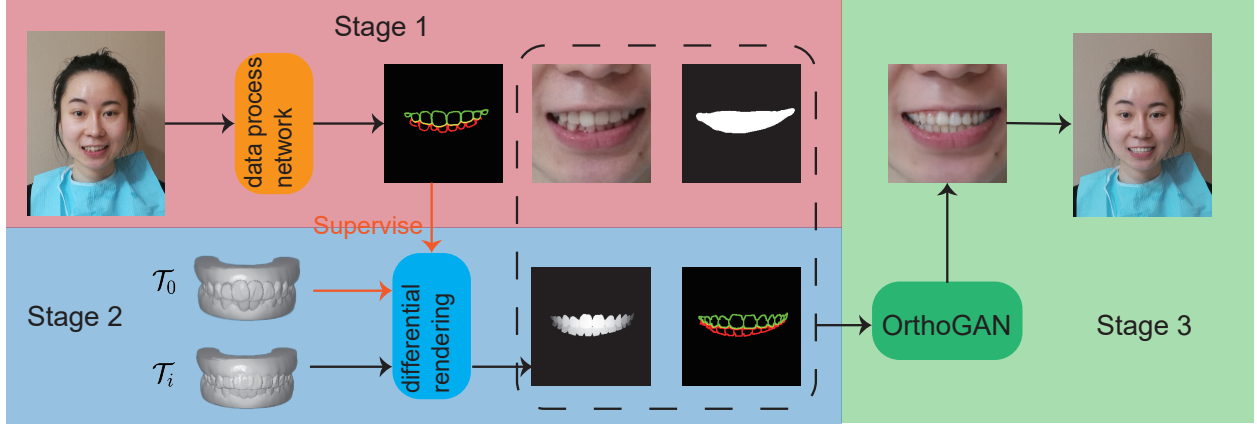


Figure 2: **Overview of our framework.** T_0 is the initial scanned model of patients’ teeth. The parameters used to render the following T_i derive from the result of the differential rendering of T_0 . The orange arrows denote the optimization of camera parameters in the fitting stage.

2.1 Differentiable Rendering

In traditional rendering, a series of parameters such as geometry, lighting, material, and camera position are passed to a rasterization or ray tracing renderer, which outputs an image after a series of pipeline operations. Due to its difficulty in reverse derivation, differentiable rendering came into being. It introduces differentiable operations in the rendering process so that it can adjust the rendering parameters through gradient backpropagation to optimize the difference between the output result and the target [72].

In recent years, differentiable rendering has been used to solve various 3D-related problems in computer vision and computer graphics, especially the reconstruction of mesh[73, 74] and texture based on mesh [96]. Supervised learning from real 3D shapes is a straightforward approach in 3D object reconstruction from images, which requires annotation of the 3D shapes corresponding to the images. Some work proposes to replace 3D annotations with 2D annotations [75, 93], which can reduce the cost of labeling 3D objects. For example, Kanazawa uses the distance of the projection of the key points of the object to reconstruct the shape of the object [76]. Bogo recovers human pose using joint point locations predicted from 2D images [77]. In addition to image key points, there are also works using 2D mask [78] and heatmap [79] as supervisory signals to assist object reconstruction more accurately. Due to the practical application of human faces in the game and animation industries, many works focus on using differentiable rendering for face reconstruction [80, 81, 82]. Wu et al. [83] proposed a fully unsupervised method to learn to reconstruct real faces from face images by exploiting shadow information. However, different from face images, the keypoints on the teeth images are much harder to precisely detected due to the scarcity of features and occlusion between the lips and teeth.

In the application of differentiable rendering, a reasonable gradient loss function is crucial. In this paper, we design a special rendering pipeline to optimize the camera pose and internal parameters by the difference of tooth edges.

2.2 Human Face Manipulation

Face editing is to change certain features of a specific face, such as changing gender [84], age[85], hair color [91], and so on, which can realize the changes of abstract faces and transform faces. It has a wide range of applications in face beautification, face prediction, and other fields. In the early days, researchers used methods based on statistics [92], based on gradient techniques [90], based on prototypes or physical models. However, these methods have certain limitations. Prototype-based methods [88] use the average difference between different attributes for mode transfer, so that the generated faces do not have individual characteristics. Physical model-based [87] methods perform parametric modeling on shape and texture, which usually requires a large number of training samples. With the development of data science, face editing is regarded as a regression problem. Jin [86] proposed a method to remove face glasses, training a linear regression model from face images with glasses and image samples without glasses, but its performance largely depends on the quality of the samples.

With the prosperity of deep learning, generative models such as GAN [6] and VAE [6] have been proposed. Through generative models, low-dimensional data is converted to a high-dimensional image data domain, and face generation is no longer difficult [67, 68, 69]. At present, the most advanced face generation models, such as BigGAN [10] and

StyleGAN [8], can already create high-resolution realistic face images that do not exist in the real world. Among the generative models for image editing, StyleGAN [8, 55] performs most prominently and is widely recognized as a model for generating high-quality faces. It introduces a style-based multi-scale generator to map images in a latent space. Encoders such as pSp [48] and e4e [66] are trained to encode target face images into latent codes for further editing. Subsequent works [70, 71] like StyleEX [94] added some constraints to edit image details, such as wrinkles, skin color, glasses, etc., which generate high-definition face images. However, there are few fine-grained local image generation and fusion, such as tooth and hair. Several previous works [98] suffer from the lack of hard control in other face regions.

Like UPHDR-GAN [97], we do not have pair images for training in this work. Compared with prior works, we focus on manipulating the mouth region of human face images and present a new generator based on StyleGAN, which can be regarded as the decoder in our encoder-decoder framework.

3 Methodology

Given a face photograph \mathcal{X} of a patient with visible misaligned teeth, the CAD model of scanned teeth \mathcal{T}_0 , the orthodontics plan the alignment treatments represented as new teeth models $\{\mathcal{T}_i\}_{i=1}^N$. Our purpose is to visualize the treatment on the teeth region in partial image x_0 while keeping other parts the same. Omitting detecting the position of x_0 in \mathcal{X} , This task can be split into two major parts: pose fitting of θ and conditional image inpainting of x_i . We denote θ as fitting parameters and x_i as the inpainting result of \mathcal{T}_i on x_0 .

3.1 Analysis of the Previous Limitation

In the former work[17], the teeth alignment visualization was formulated as:

$$\mathcal{L}(x, \theta, \phi) = \mathbb{E}_{q(z|x)}(-\log p(x | z, g)) + D_{kl}(q(z | x) || p(z)), \quad (1)$$

where θ and ϕ denote the parameters of their generative network \mathcal{N} and encoder \mathcal{M} , and D_{kl} refers to the KL divergence. This formulation is based on a strong consumption that the in-mouth appearance z is independent of the geometry g . This consumption is unreasonable because the shape of teeth influences the in-mouth appearance. Thus the simple traditional U-Net architecture without style structure in previous work [17] fails to handle this task. To circumvent this problem, the former work extract the teeth silhouette $g_y := \{g_u, g_l\}$ to independently represent the teeth geometry and utilize style-based convolution and separate encoder \mathcal{N}_{enc} to avoid the spatial attribution in z . These strategies bring new problems. First, the teeth silhouette g_y contains little information to represent teeth geometry. Second, the double-encoder synthesis network structure is unstable in some special cases and easy to collapse in the training stage. To figure out the first problem, we add a new input map to represent the geometry of the teeth: g_d , thus our g_y becomes $\{g_u, g_l, g_d\}$. The previous work [17] also mentions a similar input map in the evaluation of *TSynNet*. However, in their comparison, the output of *TSynNet* is based on well-posed teeth silhouette while the output of the control group [95] is based on wrong fitted teeth pose which we believe is unfair. This comparison also reveals to us that the pose-fitting algorithm in previous work is unreliable, even with their interactive interface. We introduce our new pose fitting algorithm and new input geometry map in Sec. 3.2. We also propose a new conditional synthesis model to replace the *TSynNet* in [17]. The structure and training method is introduced in Sec. 3.3.

3.2 Teeth Pose fitting

As shown in Fig. 1, in stage 2, we project the 3D teeth \mathcal{T}_i arranged by orthodontists to the input modalities needed in stage 3. Since the face image \mathcal{X} is not calibrated, we need to predict the parameters for camera extrinsic, intrinsic, and radial distortions. The optimized parameters θ in our work also contain the offset of lower teeth towards upper teeth. Different from other pose-fitting tasks, most teeth images in portrait exhibit all-white texture without enough RGB or depth information to fit. The occlusion from lips and bad intraoral lighting conditions also require the fitting method to be more robust. So we customize a differentiable depth shader to replace the EM algorithm in former work [17]. We render a depth image by the differentiable renderer r with our customized shader. The depth image is transferred to a teeth contour image similar to g_y within the region g_m . Since the whole render process is differentiable, we can iteratively fit the teeth position guided by the gap between g_y and the rendering result. By altering the learning rate, we can first optimize the translation matrix and then update the rotation matrix, focal length, and offset guided by the 12 loss function:

$$L_\theta := \|g_u + g_l - g_m * r_\theta(T_0)\|_2^2 \quad (2)$$

This edge-rendering-based fitting method allows us to update more parameters than previous work thus our fitting result has higher fidelity to the image X . Our edge-based optimization also circumvents the influence of inaccuracy detected keypoints in previous work. After getting the best rendering parameters, we can render teeth model \mathcal{T}_i to depth image g_d^i and transfer it to g_u^i and g_l^i with a common shader.

3.3 OrthoGAN

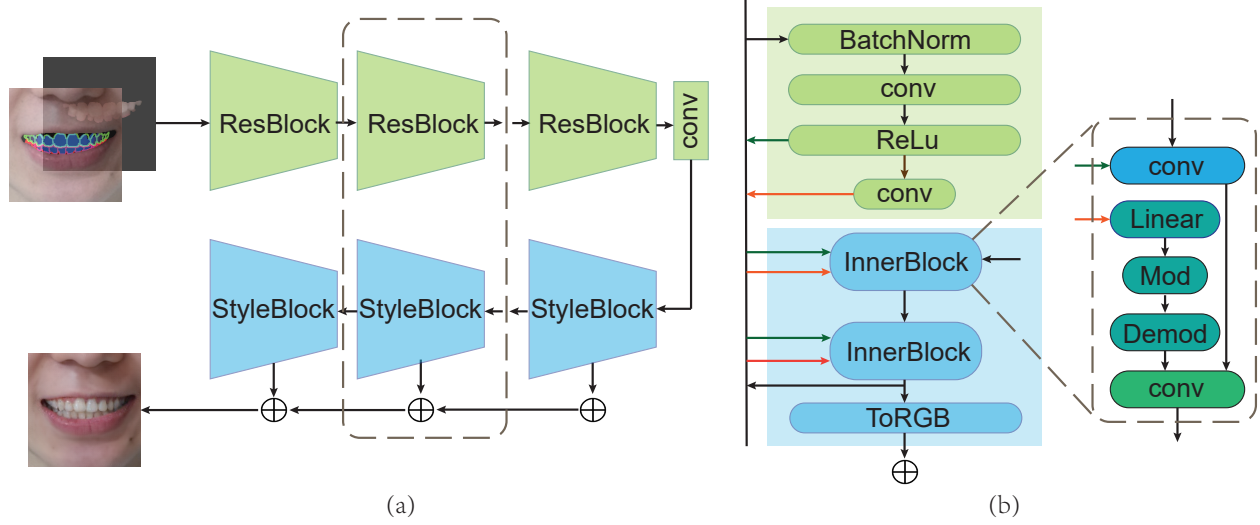


Figure 3: **The architecture of our OrthoGAN.** (a) The StyleBlock is based on the style generation structure with modulate and demodulate layers. The ResBlock and part of the StyleBlock constitute a UNet-like structure. All ResBlock formed the encoder \mathcal{E} and all StyleBlock formed the decoder \mathcal{D} . (b) The inner structure of ResBlock and StyleBlock. The middle arrows denote the transfer of the feature maps between two corresponding blocks. For simplicity, learned weights and noises of style mechanism are omitted.

OrthoGAN is a conditional synthesis network trained by adversarial, perceptual, and control loss. We apply *OrthoGAN* to generate natural images of the human face in the mouth region. To extract the geometry and visual feature from input data, our *OrthoGAN* contains an encoder \mathcal{E} which projects different input data into the latent space of decoder \mathcal{D} .

Input data. The input of *OrthoGAN* can be regarded as a 7-channel image, which is divided into a 4-channel image and a 3-channel image in the encoder \mathcal{E} . The first 4-channel image is $input_{geo} := ((1 - g_m) * x_0 + g_u + g_l + g_d) \oplus g_m$ concat with g_m and the 3-channel image is $input_{style} := g_t * x_0$ where g_t and g_m denotes the segmentation result of teeth and mouth cavity. g_u and g_l represent the edge silhouette of upper and lower teeth respectively.

Encoder \mathcal{E} . As we mentioned before, the encoder \mathcal{E} takes $input_{geo}$ and $input_{style}$ to generate the input features of decoder \mathcal{D} . When \mathcal{E} gets $input_{geo}$, the network applies an optional convolution layer to unify the channel number of $input_{geo}$. After that, the extraction module of \mathcal{E} accepts the unified image and appends the middle-generated feature in an empty list. To circumvent the influence of $(1 - g_m) * x_0$ in $input_{geo}$, we apply convolutional layers on every element in this feature list. The last element will replace our decoder’s constant input, which is built upon StyleGAN [8]. Other elements in the feature list will be added on the corresponding middle feature map before processing by the StyleConv layer in our decoder \mathcal{D} .

When \mathcal{E} meets $input_{style}$, the image is directly cast into the extraction module without the conditional convolutional layer. Different from the elements in the feature list of $input_{geo}$, the elements in the feature list of $input_{style}$ apply the average pooling and full connection layer after the convolution to minimize the geometry information in the feature map. The output feature map list can be regarded as the latent codes of the decoder \mathcal{D} to keep the style of the generated teeth image aligned with the teeth in x_0 .

Decoder \mathcal{D} . The decoder \mathcal{D} was built upon the structure of the generator of StyleGAN but it takes a 16×16 latent space instead of a constant input. As shown in Figure ref, the latent space is the feature result extracted from the $input_{geo}$ without the information from $input_{style}$. In the following blocks, the feature maps generated by $input_{geo}$ are added to the middle convolution results. The latent codes from $input_{style}$ perform convolution with added maps after passing the Mod&Demod modules. Similar to the StyleGAN, the output of the decoder \mathcal{D} is the summarization of results from to-rgb layers.

Postprocess. In both the training and testing stages, before being cast into the discriminator, the final result of OrthoGAN replaces the generated lip and skin region with the region in the original image x_0 . Then the discriminator can detect the potential inconsistency in the final result and force the OrthoGAN to learn to blend naturally in the junction of lips and teeth.

Loss function. We train the encoder \mathcal{E} and the decoder \mathcal{D} in different stage. The training of the decoder \mathcal{D} follows StyleGAN with the adversarial loss. The OrthoGAN loads the pre-trained decoder’s weight and trains the encoder with the loss:

$$\mathcal{L}_{\text{Ortho}} = \mathcal{L}_{\text{adv}} + \lambda_1 \mathcal{L}_{\text{rec}} + \lambda_2 \mathcal{L}_{\text{reg}} \quad (3a)$$

$$\mathcal{L}_{\text{rec}} = \text{LPIPS}(x_0, \hat{x}_0) + \lambda_3 \|x_0 - \hat{x}_0\|_2^2 \quad (3b)$$

where \mathcal{L}_{adv} is an adversarial loss to improve the realism. \mathcal{L}_{rec} is the reconstruction loss which contains perceptual loss and pixel loss and encourages the generated teeth to have the same appearance as the original teeth. \mathcal{L}_{reg} [48] evaluates the distance between the latent code predicted by the encoder and the average latent code.

4 Experimental Results

Datasets. We get two modal data from our collaborated medical institutions: a face photograph of a patient with visible misaligned teeth \mathcal{X} and a list of 3D teeth objects $\{T_i\}_{i=1}^k$ representing the changing of the patient’s teeth during the alignment. We evaluate our method on the dataset processed from these data. The dataset contains 2000 cases, covering a wide range of patients with different ages, genders, and teeth appearance. We use 1900 of them to train our network and select 100 cases as the test set.

Implementation details. We set $\lambda_1 = 0.01$, $\lambda_2 = 1$ and $\lambda_3 = 0.1$ in our loss functions. All networks use the Adam optimizer with learning rates = 0.0001. The decoder takes 25000 training steps and the encoder of OrthoGAN and other comparison networks takes 15000 training steps. It empirically takes 200 steps for the differentiable rendering method to fit the teeth pose. The mouth region image is set to 256×256 resolution in our experiments. All experiments run on a server with eight Nvidia 3090 GPUs, an AMD EPYC 7402 24-core processor, and 252 GB RAM.

Baselines. We evaluate our method on two aspects: (1) **Pose fitting:** we run the fitting algorithm in iOrthoPredictor [17] to show the robustness of our method. (2) **Image inpainting:** we compare the mouth image inpainting result between StyleEX [94], TSynNet in iOrthoPredictor, and our OrthoGAN. As we mentioned before, StyleEX is a simple and effective method for characterizing unaligned faces. We apply it to the inpainting task with the mask-to-face translation setting combined with the sketch-to-face translation setting. We exhibit the effectiveness of our design through ablation studies. Our pipeline can handle challenging cases while the former method fails to generate correct results.

Fitting result We randomly selected 200 patients with different ages, genders, and smile conditions as our test group. We regard 10 of them as challenging cases because of the large occlusion of lips and teeth and the offset of upper and lower teeth. We perform the point-based EM algorithm and our differentiable pose fitting on the test set. According to our statistics, the EM algorithm failed 50 cases, and 20 of them were in the challenging set. Our method failed 3 cases, and all of them were in the challenging set.

Inpainting result As shown in figure 6, some results of TSynNet have black spots on the tooth and lack natural depth, especially in the corner of the mouth. These two flaws reveal that the single silhouette of teeth fails to represent the full geometric information needed by the generation network. To prove this assumption, we remove the depth g_d in $input_{geo}$ and our OrthoGAN also shows similar black spots and teeth with unnatural depth in the corner.

Our result of OrthoGAN also shows better blending results and closer teeth color than the other two models. The better blending results contribute to the discriminator of our adversarial loss which forces the style of generated teeth to align with the lip and skin region concatenated in the post-process. In the meantime, our ablation study proves that with the same length latent code, the replacement of lip and skin regions in the post-process also helps the decoder \mathcal{D} reconstruct the color of teeth. In contrast, the inpainting task without the completed input information on lip and skin seems like an ill-posed problem in the former work [17].

Given the original teeth image x as target and the $input_{geo}$ from the initial teeth arrangement \mathcal{T}_0 , we can quantitatively evaluate the teeth visual reconstruction ability of different generation models: $\mathcal{L}_{\text{visual}} := \text{MSE}(g_m * x, g_m * \hat{x}_0)$. With a well-trained teeth edge detection network \mathcal{D} , we can statistic the edge accuracy in the generated teeth images: $\mathcal{L}_{\text{edge}} := \text{MSE}(g_l^i + g_d^i, \mathcal{D}(\hat{x}_i))$. The MSE denotes the mean squared error and \hat{x} is the generated images. We list the results in Table 1. The DR denotes that the inputs of *TSynNet* are based on the fitting results by differentiable rendering.

User study To evaluate the generation quality of the three models on teeth image inpainting, five doctors and five patients were collected to validate the simulation results of the three models. The images were evaluated in three aspects including simulation authenticity, simulation aesthetics, and image quality. The results were evaluated in a blind method

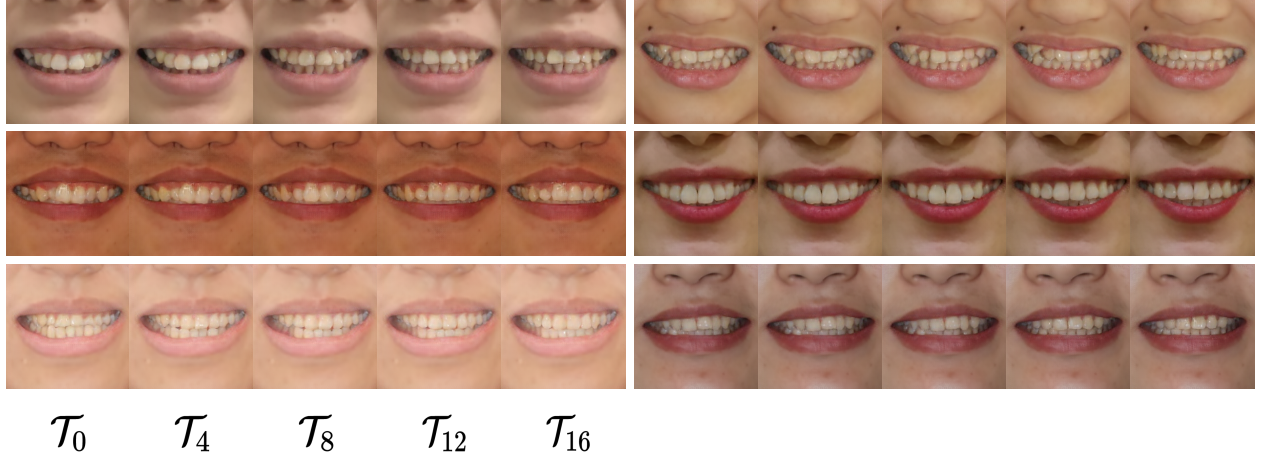


Figure 4: Dynamic inpainting results of OrthoGAN. We selected several treatment alignment visualizations with steps from \mathcal{T}_0 to \mathcal{T}_{16} , and all the alignment simulation results can form a video to illustrate the movement of the teeth.

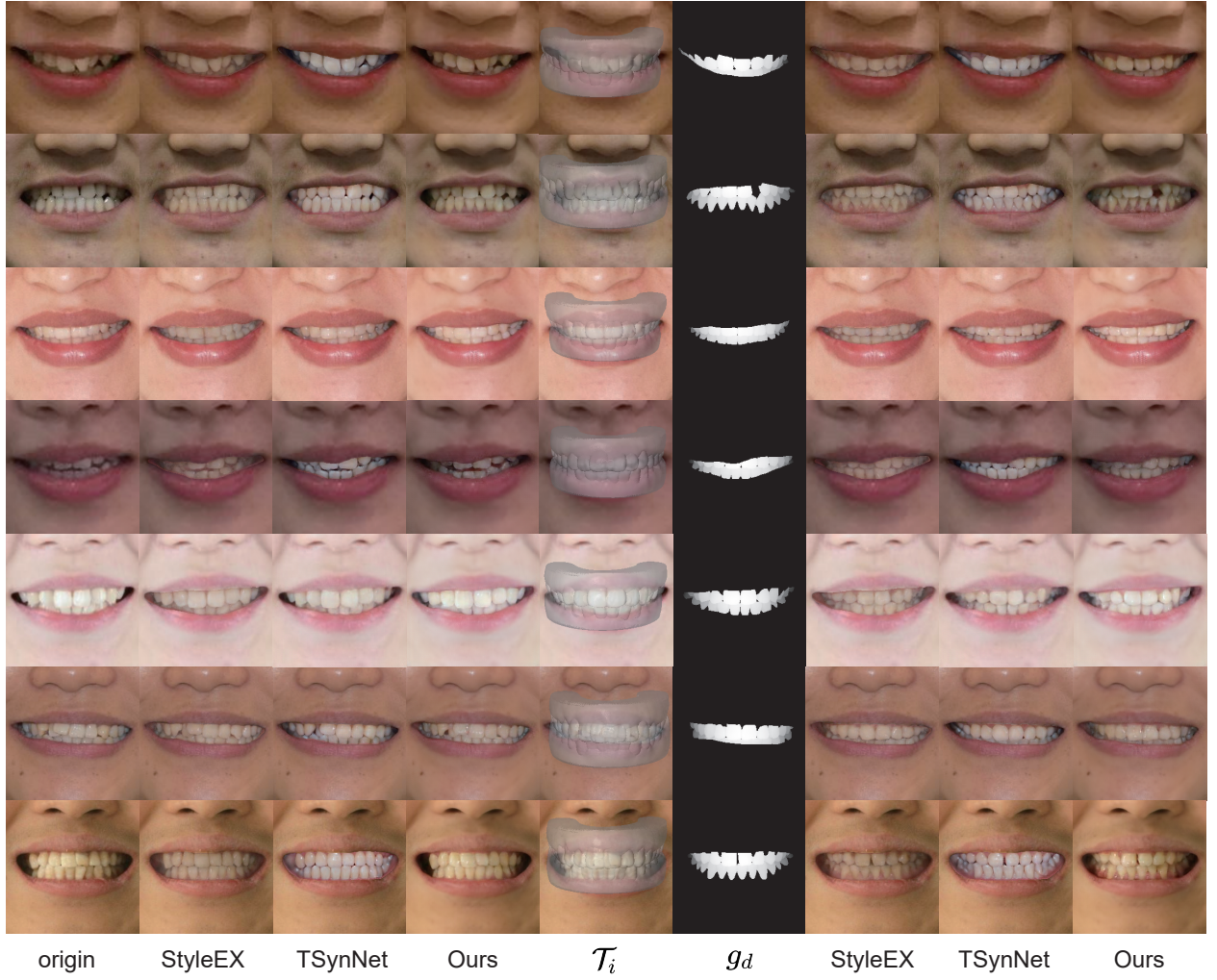


Figure 5: Comparison on origin teeth reconstruction and new alignment visualization. The first column is the original teeth image. The second, third, and fourth column is the reconstruction result from StyleEX, TSynNet, and our OrthoGAN. The fifth column is the \mathcal{T}_i and the sixth column is the rendered depth image of corresponding teeth. The seventh, eighth, and ninth column is the alignment result from StyleEX, TSynNet, and our OrthoGAN.

Table 1: Comparison of quantitative results from different frameworks on the test patient set.

	StyleEX	TSyn(DR)	Ortho w/o post	Ortho
\mathcal{L}_{edge}	0.26	0.24	0.22	0.21
\mathcal{L}_{visual}	1.01	1.01	1.00	0.86

Table 2: Scores statistics to the simulation results rated by orthodontics.

	OrthoGAN	TSynNet	StyleEX	P
Simul-authenticity	9.05±0.64	8.93±0.36	7.12±0.45	0.001
Simul-aesthetics	7.97±0.65	6.83±0.38	8.06±0.58	0.0002
Image quality	7.99±0.34	7.74±0.38	6.88±0.38	0.0005

Table 3: Scores statistics to the simulation results rated by patients.

	OrthoGAN	TSynNet	StyleEX	P
Simul-authenticity	8.03±0.36	7.95±0.37	6.91±0.45	0.004
Simul-aesthetics	7.71±0.44	6.90±0.40	7.88±0.38	0.003
Image quality	7.79±0.42	7.71±0.40	6.96±0.36	0.0002

by five doctors and five patients. The score ranges from 0 to 10 from low to high. To avoid subjective bias among different doctors and patients, we regard the average score of several patients as the final evaluation result.

The final data were shown as means (with standard deviations). Groups were compared by one-way analysis of variance, and the significance of mean difference within (intra) and between (inter) groups was performed using the PSD post hoc test after ascertaining normality by the Shapiro-Wilk test and the homogeneity of variance between groups by the Levene test. A two-tailed P value less than 0.05 ($P < 0.05$) was considered statistically significant. All analyses were performed using SPSS software (Windows version 28.0; SPSS Inc., Chicago, ILL, USA).

The evaluation results of the doctors are shown in Table 2. The scores of simulation authenticity and image quality in OrthoGAN are statistically higher than those of TSynNet and StyleEX. The simulation aesthetics of OrthoGAN and StyleEX show almost no difference but are statistically higher than that of the TSynNet. In conclusion, the OrthoGAN shows the best performance in the view of orthodontics.

The evaluation results of the patients are shown in Table 3. OrthoGAN and TSynNet show almost no difference in simulation authenticity. The scores of OrthoGAN and TSynNet in image quality were higher than StyleEX, which indicates that StyleEX shows the worst performance in the eyes of doctors and patients.



Figure 6: **Ablation experiments.** We show the generation results from the models without post-process and g_d in the $input_{geo}$.

5 Conclusion

In this study, an image was generated based on the before-treatment frontal face image and the after-orthodontics 3D teeth model. We transfer the input modalities for the quality and efficiency of image generation. In the modal transfer stage, our differentiable rendering is more efficient and precise. Our method does not rely on any preconditions and its

optimized parameters are explainable. The gradient descent which has been proven to be one of the most powerful optimizing methods [56] accelerates our rendering process and makes it a lot faster than the EM algorithm in previous work.

The most important contribution of this work is the design of our generation model: OrthoGAN. We take the single encoder architecture to form a UNet structure and stabilize the training of our network. The training of TSynNet which contains double encoders fails many times in our experiment. Previous work [17] proves that the large size of latent space helps the reconstruction of teeth geometry in the final result. However, due to the leak of visual information in the input data, they only applied the 4×4 latent space while we solved this problem and our latent space is 16×16 . The larger latent space brings more precise teeth contour in our experiment as shown in table 1. The post-process module in our OrthoGAN also helps to generate smile images with more realistic teeth including color, lighting, and perspective effects. The concatenate method forces the network to blend the lips and teeth and the latent code to focus on the appearance of the original teeth. This method can be applied to other style-based inpainting tasks. Apart from the network structure, the selection of input modalities also contributes to the exhibition. Many layers in OrthoGAN are very similar to the style-based layers in StyleEX. However, like the TSynNet, the entangled and confused input modalities lead to some obvious defects in the generated teeth image. While we should provide plenty of control information to the networks, the influence between different modalities and differences in the training and testing stages should be taken into consideration in multi-modal conditional generation tasks.

There are still some limitations to our approach. Our method only focuses on the mouth region, thus the facial growth that could alter during the orthodontic treatment is untouched. Simulation-based methods [34] may be exploited to solve this issue by considering the change of facial bones during the treatment.

On this basis, we conclude that this study proposed a high-precision visualization framework for orthodontic smile simulation. The system uses a series of image-based facial editing techniques to generate the most natural and accurate simulation results for users to date. Experiments and perceptual user studies in different settings show the effectiveness of our approach in predicting the treatment effect in digital orthodontics.

With the rapid development of image generation, our work focuses on a feasible solution to a specific problem of orthodontic alignment. It convincingly reveals that deep learning and artificial intelligence possess great potential to develop more intelligent and efficient digital dental solutions. This may be considered a promising aspect of digital orthodontics and facial image manipulation.

Acknowledgment

We strongly acknowledge the invaluable support of doctors and patients. The authors have no competing interests to declare that are relevant to the content of this article.

References

- [1] G. Power, J. Breckon, M. Sherriff, and F. McDonald, “Dolphin imaging software: an analysis of the accuracy of cephalometric digitization and orthognathic prediction,” *International journal of oral and maxillofacial surgery*, vol. 34, no. 6, pp. 619–626, 2005.
- [2] R. J. Peterman, S. Jiang, R. Johe, and P. M. Mukherjee, “Accuracy of dolphin visual treatment objective (vto) prediction software on class iii patients treated with maxillary advancement and mandibular setback,” *Progress in orthodontics*, vol. 17, no. 1, pp. 1–9, 2016.
- [3] V. Badrinarayanan, A. Kendall, and R. Cipolla, “Segnet: A deep convolutional encoder-decoder architecture for image segmentation,” *IEEE transactions on pattern analysis and machine intelligence*, vol. 39, no. 12, pp. 2481–2495, 2017.
- [4] M. Tan and Q. Le, “Efficientnet: Rethinking model scaling for convolutional neural networks,” in *International conference on machine learning*. PMLR, 2019, pp. 6105–6114.
- [5] C. Ballester, M. Bertalmio, V. Caselles, G. Sapiro, and J. Verdera, “Filling-in by joint interpolation of vector fields and gray levels,” *IEEE Transactions on Image Processing*, 2001.
- [6] I. Goodfellow, J. Pouget-Abadie, M. Mirza, B. Xu, D. Warde-Farley, S. Ozair, A. Courville, and Y. Bengio, “Generative adversarial nets,” *neural information processing systems*, 2014.
- [7] D. P. Kingma and M. Welling, “Auto-encoding variational bayes,” *arXiv: Machine Learning*, 2013.
- [8] T. Karras, S. Laine, and T. Aila, “A style-based generator architecture for generative adversarial networks,” in *Proceedings of the IEEE/CVF conference on computer vision and pattern recognition*, 2019, pp. 4401–4410.

- [9] Karras, Tero and Aila, Timo and Laine, Samuli and Lehtinen, Jaakko, “Progressive growing of gans for improved quality, stability, and variation,” *arXiv preprint arXiv:1710.10196*, 2017.
- [10] A. Brock, J. Donahue, and K. Simonyan, “Large scale gan training for high fidelity natural image synthesis,” *arXiv preprint arXiv:1809.11096*, 2018.
- [11] H. Ling, K. Kreis, D. Li, S. W. Kim, A. Torralba, and S. Fidler, “Editgan: High-precision semantic image editing,” *Advances in Neural Information Processing Systems*, vol. 34, pp. 16 331–16 345, 2021.
- [12] N. W. Kingsley, *A treatise on oral deformities as a branch of mechanical surgery*. D. Appleton, 1880.
- [13] M. B. Asbell, “A brief history of orthodontics,” *American Journal of Orthodontics and Dentofacial Orthopedics*, 1990.
- [14] C. Wu, D. Bradley, P. Garrido, M. Zollhöfer, C. Theobalt, M. H. Gross, and T. Beeler, “Model-based teeth reconstruction,” *ACM Trans. Graph.*, vol. 35, no. 6, pp. 220–1, 2016.
- [15] Z. Cui, C. Li, and W. Wang, “Toothnet: Automatic tooth instance segmentation and identification from cone beam ct images,” *computer vision and pattern recognition*, 2019.
- [16] Z. Velinov, M. Papas, D. Bradley, P. F. U. Gotardo, P. Mirdehghan, S. Marschner, J. Novák, and T. Beeler, “Appearance capture and modeling of human teeth,” *ACM Transactions on Graphics*, 2018.
- [17] L. Yang, Z. Shi, Y. Wu, X. Li, K. Zhou, H. Fu, and Y. Zheng, “Iorthopredictor: model-guided deep prediction of teeth alignment,” *ACM Transactions on Graphics (TOG)*, vol. 39, no. 6, pp. 1–15, 2020.
- [18] P. Esser, R. Rombach, and B. Ommer, “Taming transformers for high-resolution image synthesis,” *computer vision and pattern recognition*, 2021.
- [19] P. Isola, J.-Y. Zhu, T. Zhou, and A. A. Efros, “Image-to-image translation with conditional adversarial networks,” *computer vision and pattern recognition*, 2016.
- [20] W. Chen and J. Hays, “Sketchygan: Towards diverse and realistic sketch to image synthesis,” *arXiv: Computer Vision and Pattern Recognition*, 2018.
- [21] S.-Y. Chen, W. Su, L. Gao, S. Xia, and H. Fu, “Deepfacedrawing: deep generation of face images from sketches,” *ACM Transactions on Graphics*, 2020.
- [22] X. Huang, A. Mallya, T.-C. Wang, and M.-Y. Liu, “Multimodal conditional image synthesis with product-of-experts gans,” *ArXiv*, vol. abs/2112.05130, 2021.
- [23] R. Vedantam, I. Fischer, J. Huang, and K. Murphy, “Generative models of visually grounded imagination,” *Learning*, 2017.
- [24] M. Wu and N. D. Goodman, “Multimodal generative models for scalable weakly-supervised learning,” *neural information processing systems*, 2018.
- [25] W. Xia, Y. Yang, J.-H. Xue, and B. Wu, “Tedigan: Text-guided diverse face image generation and manipulation,” *arXiv: Computer Vision and Pattern Recognition*, 2020.
- [26] O. Ronneberger, P. Fischer, and T. Brox, “U-net: Convolutional networks for biomedical image segmentation,” in *International Conference on Medical image computing and computer-assisted intervention*. Springer, 2015, pp. 234–241.
- [27] J. Chen, Y. Lu, Q. Yu, X. Luo, E. Adeli, Y. Wang, L. Lu, A. L. Yuille, and Y. Zhou, “Transunet: Transformers make strong encoders for medical image segmentation,” *arXiv preprint arXiv:2102.04306*, 2021.
- [28] Z. Zhou, M. M. Rahman Siddiquee, N. Tajbakhsh, and J. Liang, “Unet++: A nested u-net architecture for medical image segmentation,” in *Deep learning in medical image analysis and multimodal learning for clinical decision support*. Springer, 2018, pp. 3–11.
- [29] Ö. Çiçek, A. Abdulkadir, S. S. Lienkamp, T. Brox, and O. Ronneberger, “3d u-net: learning dense volumetric segmentation from sparse annotation,” in *International conference on medical image computing and computer-assisted intervention*. Springer, 2016, pp. 424–432.
- [30] C. Cao, Q. Hou, and K. Zhou, “Displaced dynamic expression regression for real-time facial tracking and animation,” *international conference on computer graphics and interactive techniques*, 2014.
- [31] E. Reinhard, M. Adhikhmin, B. Gooch, and P. Shirley, “Color transfer between images,” *IEEE Computer graphics and applications*, vol. 21, no. 5, pp. 34–41, 2001.
- [32] D. L. Ruderman, T. W. Cronin, and C.-C. Chiao, “Statistics of cone responses to natural images: implications for visual coding,” *JOSA A*, vol. 15, no. 8, pp. 2036–2045, 1998.

- [33] P.-W. Wu, Y.-J. Lin, C.-H. Chang, E. Y. Chang, and S.-W. Liao, “Relgan: Multi-domain image-to-image translation via relative attributes,” in *Proceedings of the IEEE/CVF international conference on computer vision*, 2019, pp. 5914–5922.
- [34] R. M. Koch, M. Gross, F. R. Carls, D. F. von Büren, G. Fankhauser, and Y. I. H. Parish, “Simulating facial surgery using finite element models,” *international conference on computer graphics and interactive techniques*, 1996.
- [35] C. Wu, D. Bradley, P. Garrido, M. Zollhöfer, C. Theobalt, M. H. Gross, and T. Beeler, “Model-based teeth reconstruction,” *ACM Transactions on Graphics (TOG)*, vol. 35, pp. 1 – 13, 2016.
- [36] D. F. Siqueira, M. V. da Silva, P. E. G. Carvalho, and K. M. do Valle-Corotti, “The importance of the facial profile in orthodontic diagnosis and treatment planning: a patient report.” *World Journal of Orthodontics*, vol. 10, no. 4, 2009.
- [37] G. A. Bonetti, A. Alberti, C. Sartini, and S. I. Parenti, “Patients’ self-perception of dentofacial attractiveness before and after exposure to facial photographs,” *The Angle Orthodontist*, vol. 81, no. 3, pp. 517–524, 2011.
- [38] M. Varela and J. García-Camba, “Impact of orthodontics on the psychologic profile of adult patients: a prospective study,” *American Journal of Orthodontics and Dentofacial Orthopedics*, vol. 108, no. 2, pp. 142–148, 1995.
- [39] V. P. Singh and J. Sharma, “Principles of smile analysis in orthodontics-a clinical overview,” *Health Renaissance*, vol. 9, no. 1, pp. 35–40, 2011.
- [40] X. Xu, C. Liu, and Y. Zheng, “3d tooth segmentation and labeling using deep convolutional neural networks,” *IEEE transactions on visualization and computer graphics*, vol. 25, no. 7, pp. 2336–2348, 2018.
- [41] M. Arjovsky, S. Chintala, and L. Bottou, “Wasserstein generative adversarial networks,” in *International conference on machine learning*. PMLR, 2017, pp. 214–223.
- [42] M. Mirza and S. Osindero, “Conditional generative adversarial nets,” *arXiv preprint arXiv:1411.1784*, 2014.
- [43] P. K. Atrey, M. A. Hossain, A. El Saddik, and M. S. Kankanhalli, “Multimodal fusion for multimedia analysis: a survey,” *Multimedia systems*, vol. 16, no. 6, pp. 345–379, 2010.
- [44] L. Xie, C. Xiang, Z. Yu, G. Xu, Z. Yang, D. Cai, and X. He, “Pi-rcnn: An efficient multi-sensor 3d object detector with point-based attentive cont-conv fusion module,” in *Proceedings of the AAAI conference on artificial intelligence*, vol. 34, no. 07, 2020, pp. 12 460–12 467.
- [45] S. Vora, A. H. Lang, B. Helou, and O. Beijbom, “Pointpainting: Sequential fusion for 3d object detection,” in *Proceedings of the IEEE/CVF conference on computer vision and pattern recognition*, 2020, pp. 4604–4612.
- [46] A. Lugmayr, M. Danelljan, A. Romero, F. Yu, R. Timofte, and L. Van Gool, “Repaint: Inpainting using denoising diffusion probabilistic models,” in *Proceedings of the IEEE/CVF Conference on Computer Vision and Pattern Recognition*, 2022, pp. 11 461–11 471.
- [47] B. Chen, H. Fu, K. Zhou, and Y. Zheng, “Orthoaligner: Image-based teeth alignment prediction via latent style manipulation,” *IEEE Transactions on Visualization and Computer Graphics*, 2022.
- [48] E. Richardson, Y. Alaluf, O. Patashnik, Y. Nitzan, Y. Azar, S. Shapiro, and D. Cohen-Or, “Encoding in style: a stylegan encoder for image-to-image translation,” in *Proceedings of the IEEE/CVF conference on computer vision and pattern recognition*, 2021, pp. 2287–2296.
- [49] A. H. Bermano, R. Gal, Y. Alaluf, R. Mokady, Y. Nitzan, O. Tov, O. Patashnik, and D. Cohen-Or, “State-of-the-art in the architecture, methods and applications of stylegan,” in *Computer Graphics Forum*, vol. 41, no. 2. Wiley Online Library, 2022, pp. 591–611.
- [50] L. Metz, B. Poole, D. Pfau, and J. Sohl-Dickstein, “Unrolled generative adversarial networks,” *arXiv preprint arXiv:1611.02163*, 2016.
- [51] He, Kaiming and Zhang, Xiangyu and Ren, Shaoqing and Sun, Jian, “Deep residual learning for image recognition,” *Proceedings of the IEEE conference on computer vision and pattern recognition*, 2016.
- [52] Mao, Xudong and Cao, Liujuan and Gnanha, Aurele T and Yang, Zhenguo and Li, Qing and Ji, Rongrong, “Cycle Encoding of a StyleGAN Encoder for Improved Reconstruction and Editability” *arXiv preprint arXiv:2207.09367*, 2022.
- [53] Wang, Tengfei and Zhang, Yong and Fan, Yanbo and Wang, Jue and Chen, Qifeng, “High-fidelity gan inversion for image attribute editing,” *Proceedings of the IEEE/CVF Conference on Computer Vision and Pattern Recognition*, 2022.
- [54] Goodfellow, Ian and Pouget-Abadie, Jean and Mirza, Mehdi and Xu, Bing and Warde-Farley, David and Ozair, Sherjil and Courville, Aaron and Bengio, Yoshua, “Generative adversarial networks” *Communications of the ACM*, 2020.

- [55] Karras, Tero and Laine, Samuli and Aittala, Miika and Hellsten, Janne and Lehtinen, Jaakko and Aila, Timo, “Analyzing and improving the image quality of stylegan” *Proceedings of the IEEE/CVF conference on computer vision and pattern recognition*, 2020.
- [56] Ruder, Sebastian, “An overview of gradient descent optimization algorithms,” *arXiv preprint arXiv:1609.04747*, 2016.
- [57] Mildenhall, Ben and Srinivasan, Pratul P and Tancik, Matthew and Barron, Jonathan T and Ramamoorthi, Ravi and Ng, Ren, “Nerf: Representing scenes as neural radiance fields for view synthesis,” *Communications of the ACM*, 2021.
- [58] Zhang, Kai and Riegler, Gernot and Snavely, Noah and Koltun, Vladlen, “Nerf++: Analyzing and improving neural radiance fields,” *arXiv preprint arXiv:2010.07492*, 2020.
- [59] Oechsle, Michael and Peng, Songyou and Geiger, Andreas, “Unisurf: Unifying neural implicit surfaces and radiance fields for multi-view reconstruction,” *Proceedings of the IEEE/CVF International Conference on Computer Vision*, 2021.
- [60] Wang, Peng and Liu, Lingjie and Liu, Yuan and Theobalt, Christian and Komura, Taku and Wang, Wenping, “Neus: Learning neural implicit surfaces by volume rendering for multi-view reconstruction,” *arXiv preprint arXiv:2106.10689*, 2021.
- [61] Garbin, Stephan J and Kowalski, Marek and Johnson, Matthew and Shotton, Jamie and Valentin, Julien, “Fastnerf: High-fidelity neural rendering at 200fps,” *Proceedings of the IEEE/CVF International Conference on Computer Vision*, 2021.
- [62] Bian, Wenjing and Wang, Zirui and Li, Kejie and Bian, Jia-Wang and Prisacariu, Victor Adrian, “NoPe-NeRF: Optimising Neural Radiance Field with No Pose Prior,” *arXiv preprint arXiv:2212.07388*, 2022.
- [63] Wang, Zirui and Wu, Shangzhe and Xie, Weidi and Chen, Min and Prisacariu, Victor Adrian, “NeRF-: Neural radiance fields without known camera parameters,” *arXiv preprint arXiv:2102.07064*, 2021.
- [64] Müller, Thomas and Evans, Alex and Schied, Christoph and Keller, Alexander, “Instant neural graphics primitives with a multiresolution hash encoding,” *ACM Transactions on Graphics (ToG)*, 2022.
- [65] Fridovich-Keil, Sara and Yu, Alex and Tancik, Matthew and Chen, Qinhong and Recht, Benjamin and Kanazawa, Angjoo, “Instant neural graphics primitives with a multiresolution hash encoding,” *Proceedings of the IEEE/CVF Conference on Computer Vision and Pattern Recognition*, 2022.
- [66] Tov, Omer and Alaluf, Yuval and Nitzan, Yotam and Patashnik, Or and Cohen-Or, Daniel, “Designing an encoder for stylegan image manipulation,” *ACM Transactions on Graphics (TOG)*, 2021.
- [67] Dhariwal, Prafulla and Nichol, Alexander, “Diffusion models beat gans on image synthesis,” *Advances in Neural Information Processing Systems*, 2021.
- [68] Karras, Tero and Aittala, Miika and Aila, Timo and Laine, Samuli, “Elucidating the design space of diffusion-based generative models,” *arXiv preprint arXiv:2206.00364*, 2022.
- [69] Ho, Jonathan and Salimans, Tim and Gritsenko, Alexey and Chan, William and Norouzi, Mohammad and Fleet, David J, “Video diffusion models,” *arXiv preprint arXiv:2204.03458*, 2022.
- [70] Abdal, Rameen and Qin, Yipeng and Wonka, Peter, “Image2stylegan: How to embed images into the stylegan latent space?,” *Proceedings of the IEEE/CVF International Conference on Computer Vision*, 2019.
- [71] Liu, Feng-Lin and Chen, Shu-Yu and Lai, Yukun and Li, Chunpeng and Jiang, Yue-Ren and Fu, Hongbo and Gao, Lin, “DeepFaceVideoEditing: Sketch-based deep editing of face videos,” *ACM Transactions on Graphics*, 2022.
- [72] Kato, Hiroharu and Beker, Deniz and Morariu, Mihai and Ando, Takahiro and Matsuoka, Toru and Kehl, Wadim and Gaidon, Adrien, “Differentiable rendering: A survey,” *arXiv preprint arXiv:2006.12057*, 2020.
- [73] Jiang, Boyi and Hong, Yang and Bao, Hujun and Zhang, Juyong, “Selfrecon: Self reconstruction your digital avatar from monocular video,” *Proceedings of the IEEE/CVF Conference on Computer Vision and Pattern Recognition*, 2022.
- [74] Deng, Xi and Luan, Fujun and Walter, Bruce and Bala, Kavita and Marschner, Steve, “Reconstructing translucent objects using differentiable rendering,” *ACM SIGGRAPH 2022 Conference Proceedings*, 2022.
- [75] Wu, Jiajun and Wang, Yifan and Xue, Tianfan and Sun, Xingyuan and Freeman, Bill and Tenenbaum, Josh, “Marrnet: 3d shape reconstruction via 2.5 d sketches,” *Advances in neural information processing systems*, 2017.
- [76] Yu, Alex and Ye, Vickie and Tancik, Matthew and Kanazawa, Angjoo, “pixelnerf: Neural radiance fields from one or few images,” *Proceedings of the IEEE/CVF conference on computer vision and pattern recognition*, 2021.

- [77] Hasson, Yana and Tekin, Bugra and Bogo, Federica and Laptev, Ivan and Pollefeys, Marc and Schmid, Cordelia, “Leveraging photometric consistency over time for sparsely supervised hand-object reconstruction,” *Proceedings of the IEEE/CVF conference on computer vision and pattern recognition*, 2020.
- [78] Baek, Seungryul and Kim, Kwang In and Kim, Tae-Kyun, “Pushing the envelope for rgb-based dense 3d hand pose estimation via neural rendering,” *Proceedings of the IEEE/CVF Conference on Computer Vision and Pattern Recognition*, 2019.
- [79] Zhang, Baowen and Wang, Yangang and Deng, Xiaoming and Zhang, Yinda and Tan, Ping and Ma, Cuixia and Wang, Hongan, “Interacting two-hand 3d pose and shape reconstruction from single color image,” *Proceedings of the IEEE/CVF International Conference on Computer Vision*, 2021.
- [80] Yu, Heng and Milacski, Zoltan A and Jeni, László A, “Unsupervised Style-based Explicit 3D Face Reconstruction from Single Image,” *Proceedings of the IEEE/CVF Conference on Computer Vision and Pattern Recognition*, 2023.
- [81] Wang, Yuxing and Lu, Yawen and Xie, Zhihua and Lu, Guoyu, “Deep Unsupervised 3D SfM Face Reconstruction Based on Massive Landmark Bundle Adjustment,” *Proceedings of the 29th ACM International Conference on Multimedia*, 2021.
- [82] Papantoniou, Foivos Paraperas and Lattas, Alexandros and Moschoglou, Stylianos and Zafeiriou, Stefanos, “Relightify: Relightable 3D Faces from a Single Image via Diffusion Models,” *arXiv preprint arXiv:2305.06077*, 2023.
- [83] Wu, Shangzhe and Rupperecht, Christian and Vedaldi, Andrea, “Unsupervised learning of probably symmetric deformable 3d objects from images in the wild,” *Proceedings of the IEEE/CVF conference on computer vision and pattern recognition*, 2020.
- [84] Shen, Yujun and Gu, Jinjin and Tang, Xiaoou and Zhou, Bolei, “Interpreting the latent space of gans for semantic face editing,” *Proceedings of the IEEE/CVF conference on computer vision and pattern recognition*, 2020.
- [85] Yao, Xu and Puy, Gilles and Newson, Alasdair and Gousseau, Yann and Hellier, Pierre, “High resolution face age editing,” *2020 25th International conference on pattern recognition (ICPR)*, 2021.
- [86] Jin, Jesse S and Xu, Changsheng and Xu, Min and Zhang, Zhigang and Peng, Yu, “Eyeglasses removal from facial image based on mvlr,” *The Era of Interactive Media*, 2013.
- [87] Aizawa, Kiyoharu and Huang, Thomas S, “Model-based image coding advanced video coding techniques for very low bit-rate applications,” *Proceedings of the IEEE*, 1995.
- [88] Rowland, Duncan A and Perrett, David I, “Manipulating facial appearance through shape and color,” *IEEE computer graphics and applications*, 1995.
- [89] Zhang, Lvmin and Rao, Anyi and Agrawala, Maneesh, “Adding conditional control to text-to-image diffusion models,” *Proceedings of the IEEE/CVF International Conference on Computer Vision*, 2023.
- [90] Yu, Yizhou and Zhou, Kun and Xu, Dong and Shi, Xiaohan and Bao, Hujun and Guo, Baining and Shum, Heung-Yeung, “Mesh editing with poisson-based gradient field manipulation,” *ACM SIGGRAPH 2004 Papers*, 2004.
- [91] Wei, Tianyi and Chen, Dongdong and Zhou, Wenbo and Liao, Jing and Tan, Zhentao and Yuan, Lu and Zhang, Weiming and Yu, Nenghai, “Hairclip: Design your hair by text and reference image,” *Proceedings of the IEEE/CVF Conference on Computer Vision and Pattern Recognition*, 2022.
- [92] Terada, Takuma and Fukui, Takayuki and Igarashi, Takanori and Nakao, Keisuke and Kashimoto, Akio and Chen, Yen-Wei, “Automatic facial image manipulation system and facial texture analysis,” *2009 Fifth International Conference on Natural Computation*, 2009.
- [93] Ramakrishna, Varun and Kanade, Takeo and Sheikh, Yaser, “Reconstructing 3d human pose from 2d image landmarks,” *Computer Vision—ECCV 2012: 12th European Conference on Computer Vision, Florence, Italy, October 7-13, 2012, Proceedings, Part IV 12*, 2012.
- [94] Yang, Shuai and Jiang, Liming and Liu, Ziwei and Loy, Chen Change, “StyleGANEX: StyleGAN-Based Manipulation Beyond Cropped Aligned Faces,” *arXiv preprint arXiv:2303.06146*, 2023.
- [95] Xie, Saining and Tu, Zhuowen, “Holistically-nested edge detection,” *Proceedings of the IEEE international conference on computer vision*, 2015.
- [96] Lin, Lixiang and Zhu, Jianke and Zhang, Yisu, “Multiview textured mesh recovery by differentiable rendering,” *IEEE Transactions on Circuits and Systems for Video Technology*, 2022.

- [97] Li, Ru and Wang, Chuan and Wang, Jue and Liu, Guanghui and Zhang, Heng-Yu and Zeng, Bing and Liu, Shuaicheng, “Uphdr-gan: Generative adversarial network for high dynamic range imaging with unpaired data,” *IEEE Transactions on Circuits and Systems for Video Technology*, 2022.
- [98] Liu, Yunfan and Li, Qi and Deng, Qiyao and Sun, Zhenan, “Towards spatially disentangled manipulation of face images with pre-trained StyleGANs,” *IEEE Transactions on Circuits and Systems for Video Technology*, 2022.
- [99] Wang, Chao and Shao, Mingwen and Meng, Deyu and Zuo, Wangmeng, “Dual-pyramidal image inpainting with dynamic normalization,” *IEEE Transactions on Circuits and Systems for Video Technology*, 2022.
- [100] Luo, Yu and You, Bijia and Yue, Guanghui and Ling, Jie, “Pseudo-supervised low-light image enhancement with mutual learning,” *IEEE Transactions on Circuits and Systems for Video Technology*, 2023.